

1 **Photocatalytic production of bisabolene from green microalgae mutant: process analysis**  
2 **and kinetic modelling**

3  
4 Irina Harun<sup>a,‡</sup>, Ehecatl Antonio Del Rio-Chanona<sup>a,b,‡</sup>, Jonathan L. Wagner<sup>a,f</sup>, Kyle J. Lauersen<sup>e</sup>,  
5 Dongda Zhang<sup>a,b,c,d,\*</sup>, Klaus Hellgardt<sup>a,\*</sup>

6  
7 *<sup>a</sup>Department of Chemical Engineering, Imperial College London, South Kensington, United*  
8 *Kingdom, SW7 2AZ*

9  
10 *<sup>b</sup>Centre for Process Systems Engineering, Imperial College London, South Kensington*  
11 *Campus, London SW7 2AZ, UK*

12  
13 *<sup>c</sup>School of Chemical Engineering and Analytical Science, The University of Manchester,*  
14 *Oxford Road, Manchester, M1 3BU, UK*

15  
16 *<sup>d</sup>Centre for Process Integration, The University of Manchester, Oxford Road, Manchester, M1*  
17 *3BU, UK*

18  
19 *<sup>e</sup>Faculty of Biology, Bielefeld University, Universitätsstraße 25, 33615 Bielefeld, Germany*

20  
21 *<sup>f</sup>Department of Chemical Engineering, University of Loughborough, Loughborough, LE11*  
22 *3TU, UK*

23 *Tel: +44 (0) 1509 222546*

24 *‡: These authors contributed equally to this work.*

25  
26 *\*: corresponding authors, email: [dongda.zhang@manchester.ac.uk](mailto:dongda.zhang@manchester.ac.uk) (Dongda Zhang);*  
27 *[k.hellgardt@imperial.ac.uk](mailto:k.hellgardt@imperial.ac.uk) (Klaus Hellgardt).*

28  
29

## Abstract

30  
31 Currently, algal fuel research has commenced to shift towards genetically engineered mutants,  
32 able to express and excrete desired products directly into the culture. In this study, a mutant  
33 strain of *Chlamydomonas reinhardtii*, engineered for bisabolene (alternative biodiesel)  
34 excretion, was cultivated at different illumination and temperatures to investigate their effects  
35 on cell growth and bisabolene production. Moreover, a kinetic model was constructed to  
36 identify the desirable conditions for biofuel synthesis. Three original contributions were  
37 concluded. Firstly, this work confirmed that bisabolene was partially synthesised  
38 independently of biomass growth, indicating its feasibility for continuous production.  
39 Secondly, it was found that whilst bisabolene synthesis was independent of light intensity, it  
40 was strongly affected by temperature, resulting in conflicting desirable conditions for cell  
41 growth and product synthesis. Finally, through model prediction, optimal operating conditions  
42 were identified for mutant growth and bisabolene synthesis. This study therefore paves the way  
43 towards chemostat production and process scale-up.

44

45 **Keywords:** Photocatalysis; Kinetic modelling; Photobioreactor; Excreted biofuels; Process  
46 optimisation.

## 47 **Introduction**

48 Autotrophic organisms such as microalgae and cyanobacteria have long been regarded as  
49 highly promising feedstocks for the production of third-generation biofuels. These organisms  
50 display rapid growth rates and require minimal input of trace elements, using light to harvest  
51 CO<sub>2</sub> as the sole carbon source<sup>1-4</sup>. However, commercial progress of algae derived biofuels has  
52 been slow, limited by the high costs of algae cultivation, harvesting, and downstream  
53 processing. Current production facilities are based around the cultivation of oleaginous strains  
54 for algal lipids, which are subsequently solvent-extracted and converted into biodiesel via  
55 transesterification and hydrotreatment<sup>5</sup>. An alternative approach is the hydrothermal  
56 liquefaction of the whole, wet biomass-culture to produce crude bio-oils for further upgrading  
57 into fuels<sup>6,7</sup>. Although these technologies are relatively well established and produce fuels  
58 compatible with the existing transport infrastructure, they are inefficient and costly<sup>8</sup>.

59 Consequently, engineering microalgae and cyanobacteria to excrete desired products directly  
60 into the culture medium is a highly desired solution to overcome the limitations of conventional  
61 solvent extraction concepts. Secretion, or excretion, enables straightforward and efficient  
62 recovery of a desired (fuel) product separate from the valuable algal biomass, which can be  
63 used for any number of alternative applications or recycled within the reactor. In this way, the  
64 cells effectively act as a photo-catalyst or green-cell factory, converting light, CO<sub>2</sub> and water  
65 into a desired product. To date, the production and excretion of a number of products has  
66 already been successfully demonstrated, including free fatty acids<sup>9</sup>, alcohols, *e.g.* ethanol<sup>10</sup>,  
67 isopropanol<sup>11</sup> or butanol, and terpenoids, such as farnasene<sup>12</sup>, limonene<sup>13</sup>, and patchoulol<sup>14</sup>.

68 Terpenoids are particularly interesting targets for microbial photobiocatalysis as some have  
69 favourable fuel properties, but are produced in their native hosts to only low titres <sup>15</sup>. For  
70 example, the sesquiterpene (C15) (*E*)- $\alpha$ -bisabolene (hereafter bisabolene) is natively produced  
71 in the grand fir, *Abies grandis* <sup>16</sup>, and can be hydrogenated into bisabolane, which has  
72 particularly attractive properties as a diesel-like drop-in fuel <sup>17</sup>. Green algae and cyanobacteria  
73 are considered to be valuable hosts for terpenoid production as their native metabolism is  
74 structured to produce terpenoid molecules by the methylerythritol phosphate pathway (MEP)  
75 from glyceraldehyde-3-phosphate (G3P) and pyruvate <sup>18</sup>, representing ~5% of cellular carbon  
76 flux <sup>19</sup>. Genetically modified strains of *Synechococcus* sp. PCC 7002 were previously shown  
77 to produce bisabolene up to 0.6 mg L<sup>-1</sup> after 96 h <sup>20</sup>. Very recently, *Chlamydomonas reinhardtii*  
78 was also engineered to produce and excrete bisabolene up to 8 mg L<sup>-1</sup> in 96 h <sup>21</sup>.

79 To facilitate process scale-up, it is vital to understand effects of environmental conditions on  
80 terpenoid synthesis in photobioreactors (PBRs). A PBR is an enclosed reactor system in which  
81 illumination and nutrients are provided to facilitate algae biomass growth and biorenewables  
82 synthesis. Both light and temperature are known to have strong influences on algal productivity  
83 as well as metabolic partitioning of native products. For example, commercial production of  
84 terpenoid derived pigments (*e.g.*  $\beta$ -carotene and astaxanthin) from green algae uses high light  
85 conditions to hyper-accumulate these photo-protective carotenoids <sup>22</sup>. As bisabolene is a  
86 heterologous terpenoid product for the green algal cell, it is necessary to characterise and  
87 generate kinetic models for its production optimisation. Therefore, in this paper, a mutant strain  
88 of the green microalgae, *C. reinhardtii*, genetically modified to enable the secretion of

89 bisabolene, are utilised to investigate the effect of light intensities and temperatures on cell  
90 growth and bisabolene production. A kinetic model was constructed for the first time to  
91 simulate the influence of these key operating conditions, with the aim to investigate the  
92 biochemical reaction mechanisms and predict the optimal operating conditions for the excreted  
93 biofuel synthesis.

## 94 **Materials and methods**

### 95 **Microalgal strain and its preculture conditions**

96 The experiments were conducted with a strain of *Chlamydomonas reinhardtii* UVM4<sup>23</sup>  
97 genetically engineered with the bisabolene synthase gene (*Abies grandis* bisabolene synthase  
98 Uniprot: O81086). The strain was generated from single transformation of vector ii as  
99 described in Wichmann et al. (2018)<sup>21</sup>, and was obtained from the Kruse group at Bielefeld  
100 University. The cultures were grown in the Tris-acetate phosphate (TAP) growth medium<sup>24</sup>,  
101 using a modified trace metal solution to yield final concentrations of 20.5  $\mu\text{M}$   $\text{FeCl}_3 \cdot 6\text{H}_2\text{O}$ ,  
102 2.5  $\mu\text{M}$   $\text{ZnSO}_4 \cdot 7\text{H}_2\text{O}$ , 2.0  $\mu\text{M}$   $\text{CuSO}_4 \cdot 5\text{H}_2\text{O}$ , 6.5  $\mu\text{M}$   $\text{MnCl}_2 \cdot 4\text{H}_2\text{O}$ , 0.2  $\mu\text{M}$   
103  $(\text{NH}_4)_6\text{Mo}_7\text{O}_{24} \cdot 4\text{H}_2\text{O}$  and 57.5  $\mu\text{M}$   $\text{Na}_2\text{EDTA} \cdot 2\text{H}_2\text{O}$ .

### 104 **Operation of photobioreactor**

105 Growth experiments were conducted in a 1 L vertical flat-plate bioreactor, constructed from  
106 polymethyl methacrylate, as described previously<sup>25</sup>. The system consists of a 1 L growth  
107 chamber, illuminated by a cool white LED array and maintained at constant temperature via a  
108 secondary heating water compartment. The employed cultivation temperatures ranged from 22  
109  $^{\circ}\text{C}$  to 32  $^{\circ}\text{C}$ , with incident light intensities ranging from 20  $\mu\text{E}$  to 300  $\mu\text{E}$ . Temperature, pH and

110 light transmission probes provided constant monitoring of the culture conditions, while a  
111 sampling port at the bottom of the reactor allowed regular withdrawal of culture samples for  
112 external analysis. Mixing and the addition of atmospheric CO<sub>2</sub> was provided using filtered air  
113 bubbled continuously through a tubular sparger.

#### 114 **Analytical procedures**

115 ***Growth monitoring:*** The system temperature was continuously monitored using the  
116 thermocouple and the water bath temperature was adjusted manually to obtain the desired  
117 cultivation temperature. Dry weight measurements of culture samples were conducted using  
118 vacuum filtration of 10 mL of culture (Millipore membrane filters, 5.0 µm small molecular  
119 weight protein), followed by drying at 60 °C to constant weight. To continuously monitor  
120 biomass growth, the light transmission probe readings were used to back-calculate biomass dry  
121 weight, after calibration with the sampled dry weight readings. The pH was obtained from the  
122 internal electrode, calibrated by three-point calibration at pH 4.0, 7.0 and 10.0.

123 ***Measurement of bisabolene concentration:*** Bisabolene was extracted from 10 mL whole  
124 culture samples using 2 mL of dodecane. The organic phase was directly analysed on a Hewlett  
125 Packard 5890 gas chromatograph with an Agilent HP-5 column (50 m, 0.32 mm x 0.25 µm)  
126 and a flame ionisation detector (FID). 1 µL samples were injected at 250 °C in splitless mode  
127 using a nitrogen carrier gas flowrate of 1 ml min<sup>-1</sup>. The initial oven temperature was 80 °C,  
128 held for 1 min, followed by ramping at 10 °C min<sup>-1</sup> from 80 °C to 120 °C, 3 °C min<sup>-1</sup> from  
129 120 °C to 160 °C and again 10 °C min<sup>-1</sup> from 160 °C to 270 °C, with a final hold time of 2 min.

130 Bisabolene concentrations were quantified using standard calibration curves for bisabolene  
131 (Alfa Aesar, bisabolene, mixture of isomers).

## 132 **Model construction methodology**

133 ***Simulation of biomass growth:*** Algal biomass growth is under nutrient-sufficient conditions  
134 due to the presence of multiple carbon nutrients including acetate and CO<sub>2</sub>. The Logistic model  
135 (Equation 1) was therefore adopted in this work as it has been widely used to simulate  
136 microorganism cell growth under such conditions for both traditional fermentation processes  
137 <sup>26</sup> and microalgae photo-production systems <sup>27</sup>. In this equation, the first term on the right  
138 denotes biomass growth rate, and the second term denotes algae decay rate.

$$139 \frac{dX}{dt} = \mu \cdot X \cdot \left(1 - \frac{X}{X_{\max}}\right) = \mu \cdot X - \mu_d \cdot X^2 \quad (1)$$

140 where  $X$  is biomass concentration,  $\mu$  is biomass specific growth rate,  $X_{\max}$  is maximum  
141 biomass concentration, and  $\mu_d$  is biomass specific decay rate. Units of parameters are listed  
142 in Table 3.

143 ***Simulation of light intensity and temperature effects on algal growth:*** To account for the  
144 effects of cultivation conditions on biomass growth, the biomass specific growth rate,  $\mu$ , was  
145 expanded to include factors for light intensity and temperature (Equation 2a). These were  
146 estimated from the Aiba model (Equation 2b) and an Arrhenius-type equation (Equation 2c),  
147 respectively, commonly used for the modelling of green algae biomass <sup>28</sup>. The specific version  
148 of the Arrhenius equation was selected based on its higher accuracy compared to the other  
149 Arrhenius equation derived models derived for microorganism growth <sup>28,29</sup> and transformed  
150 further into Equation 2d to facilitate system identification.

151  $\mu = \mu_m \cdot k(I) \cdot k(T)$  (2a)

152  $k(I) = \frac{I(z)}{I(z) + k_s + \frac{I(z)^2}{k_i}}$  (2b)

153  $k(T) = A_c \cdot \exp\left[-\frac{E_a}{RT}\right] - A_d \cdot \exp\left[-\frac{E_b}{RT}\right]$  (2c)

154  $k(T) = \exp\left[-\left(\frac{E_a}{RT} - \frac{E_a}{RT_a}\right)\right] - \exp\left[-\left(\frac{E_b}{RT} - \frac{E_b}{RT_b}\right)\right]$  (2d)

155 where  $\mu_m$  is maximum biomass specific growth rate,  $I(z)$  is local light intensity,  $k_s$  is the  
 156 photosaturation term,  $k_i$  is the photoinhibition term,  $A_c$  and  $A_d$  are pre-exponential  
 157 parameters,  $E_a$  is the algae activation energy,  $E_b$  is the algae deactivation energy,  $T$  is the  
 158 culture temperature,  $T_a$  and  $T_b$  are reference temperatures, and  $R$  is the gas constant.

159 **Simulation of light attenuation in a PBR:** Effects of light attenuation within the PBR, caused  
 160 by algae cell absorption and bubble scattering<sup>30</sup>, were modelled by embedding the modified  
 161 Lambert-Beer's law into the current kinetic model (Equation 3). To prevent the complexity of  
 162 modelling the resulting partial differential equation (PDE), constituting both spatial and  
 163 temporal dimensions which limits the model's further applicability to real-time dynamic  
 164 optimisation in fed-batch and continuous processes, a 10-step Trapezoidal rule was applied to  
 165 eliminate the spatial dimension (Equation 4).

166  $I(z) = I_0 \cdot \exp[-(\tau \cdot X + K_a) \cdot z]$  (3)

167  $k(I) = \frac{1}{20} \cdot \sum_{n=1}^9 \left( \frac{I_{i=0}}{I_{i=0} + k_s + \frac{I_{i=0}^2}{k_i}} + 2 \cdot \frac{I_{i=\frac{n \cdot L}{10}}}{I_{i=\frac{n \cdot L}{10}} + k_s + \frac{I_{i=\frac{n \cdot L}{10}}^2}{k_i}} + \frac{I_{i=L}}{I_{i=L} + k_s + \frac{I_{i=L}^2}{k_i}} \right)$  (4)



168 where  $I_0$  is incident light intensity,  $\tau$  is algal cell absorption coefficient,  $K_a$  is the bubble  
 169 scattering coefficient,  $z$  is the distance from light source,  $L$  is the width of the PBR, and  $I_i$   
 170 is the local light intensity at a distance of  $i = \frac{n \cdot L}{10}$  from the PBR front exposure surface.

171 ***Simulation of bisabolene production:*** To simulate bisabolene synthesis, the Luedeking–Piret  
 172 model is applied and modified in this work<sup>31</sup>. The original Luedeking–Piret model is presented  
 173 in Equation 5a, where the first term on the right denotes the cell growth related bisabolene  
 174 production and the second term represents the growth independent bisabolene production.  
 175 Despite the original model being able to capture the kinetics of most bacterial fermentation  
 176 processes, it assumes that effects of light intensity and temperature on bioproducts synthesis  
 177 are equal to those on microalgae biomass growth, Nonetheless, for most of the currently  
 178 explored algal bioproducts *e.g.* hydrogen, astaxanthin and phycocyanin, previous studies have  
 179 declared that optimal operating conditions for these bioproducts synthesis are different or even  
 180 conflicting from those for algae cell growth<sup>32–34</sup>. Therefore, to accurately simulate bisabolene  
 181 production, the original Luedeking–Piret model is modified to Equation 5b based on the current  
 182 experimental observation and analysis. The detailed explanation for this modification is  
 183 presented in the Results and Discussion section.

$$184 \quad \frac{dP}{dt} = Y_1 \cdot \frac{dX}{dt} + Y_2 \cdot X \quad (5a)$$

$$185 \quad \frac{dP}{dt} = \left( Y_1 \cdot \frac{dX}{dt} + Y_2 \cdot X \right) \cdot \left( \alpha - \left( \exp \left[ - \left( \frac{E_a}{RT} - \frac{E_a}{RT_a} \right) \right] - \exp \left[ - \left( \frac{E_b}{RT} - \frac{E_b}{RT_b} \right) \right] \right) \right) \quad (5b)$$

186 where  $P$  is bisabolene production,  $Y_1$  is biomass growth associated bisabolene yield  
 187 coefficient,  $Y_2$  is biomass growth independent bisabolene yield coefficient, and  $\alpha$  is a  
 188 temperature related dimensionless modification parameter for bisabolene synthesis rate.

189 **Experimental data selection:** To guarantee the high accuracy and predictive capability of the  
 190 current model, four sets of experimental data were used for dynamic model parameter  
 191 estimation, with another four datasets obtained from experiments operated at conditions  
 192 different from the previous four experiments used for model verification (Table 1).

193 Table 1: Operating conditions of experiments for parameter estimation and model prediction

| Experiments for model fitting (parameter estimation)     |                                       |  |                                       |                                       |
|--|---------------------------------------|--|---------------------------------------|---------------------------------------|
|  | Experiment 1                          | Experiment 2                           | Experiment 3                          | Experiment 4                          |
| Light intensity  | 20 $\mu\text{E m}^{-2} \text{s}^{-1}$ | 300 $\mu\text{E m}^{-2} \text{s}^{-1}$ | 60 $\mu\text{E m}^{-2} \text{s}^{-1}$ | 60 $\mu\text{E m}^{-2} \text{s}^{-1}$ |
| Temperature  | 30 °C                                 | 30 °C                                  | 26 °C                                 | 32 °C                                 |
| Experiments for model predictive capability verification |                                       |  |                                       |                                       |
|  | Test 1                                | Test 2                                 | Test 3                                | Test 4                                |
| Light intensity  | 40 $\mu\text{E m}^{-2} \text{s}^{-1}$ | 100 $\mu\text{E m}^{-2} \text{s}^{-1}$ | 60 $\mu\text{E m}^{-2} \text{s}^{-1}$ | 60 $\mu\text{E m}^{-2} \text{s}^{-1}$ |
| Temperature  | 30 °C                                 | 30 °C                                  | 28 °C                                 | 22 °C                                 |

194 **Parameter estimation methodology**

195 An accurate parameter estimation framework is crucial to guarantee the accuracy and  
 196 predictive power of the developed dynamic model. Given the high accuracy of measurement  
 197 instruments and the assumption that measurement noise follows a normal distribution, a  
 198 weighted nonlinear least squares optimisation problem is formulated to determine the optimal  
 199 set of parameters that identify the system. Because of the nonlinearity and stiffness of the DAE  
 200 model, stiff system integration methods are required, and hence orthogonal collocation over  
 201 finite elements in time using Radau roots was used<sup>35</sup>. This method has proven to be highly

202 efficient for discretising dynamic systems, and computational costs are reduced significantly  
 203 compared to simpler discretisation schemes (*e.g.* implicit Euler method) <sup>36</sup>. The parameter  
 204 estimation problem in an orthogonal collocation formulation is presented in Equations 6a-h.

$$205 \quad \min_{p,x} \sum_{i=1}^N (\hat{x}_i - x(t_i, p))^T \alpha_i (\hat{x}_i - x(t_i, p)) \quad (6a)$$

206 subject to:

207 *process dynamics*

$$208 \quad \dot{x}_{i,j} = f(x_{i,j}, \dot{x}_{i,j}, p) \quad (6b)$$

209 *collocation constraints*

$$210 \quad x_{i,j} = x_{i-1,K} + h_i \sum_{l=1}^K \varphi_l(\tau_j) \dot{x}_{i,l} \quad (6c)$$

211 *continuity constraints*

$$212 \quad x_{i,0} = x_{i-1,K} \quad (6d)$$

213 *initial conditions*

$$214 \quad x_{1,0}(t_0) = x_0 \quad (6e)$$

215 *integration horizon*

$$216 \quad 0 \leq t \leq t_f \quad (6f)$$

217 *bounds*

$$218 \quad x_{lb} \leq x \leq x_{ub} \quad (6g)$$

$$219 \quad p_{lb} \leq p \leq p_{ub} \quad (6h)$$

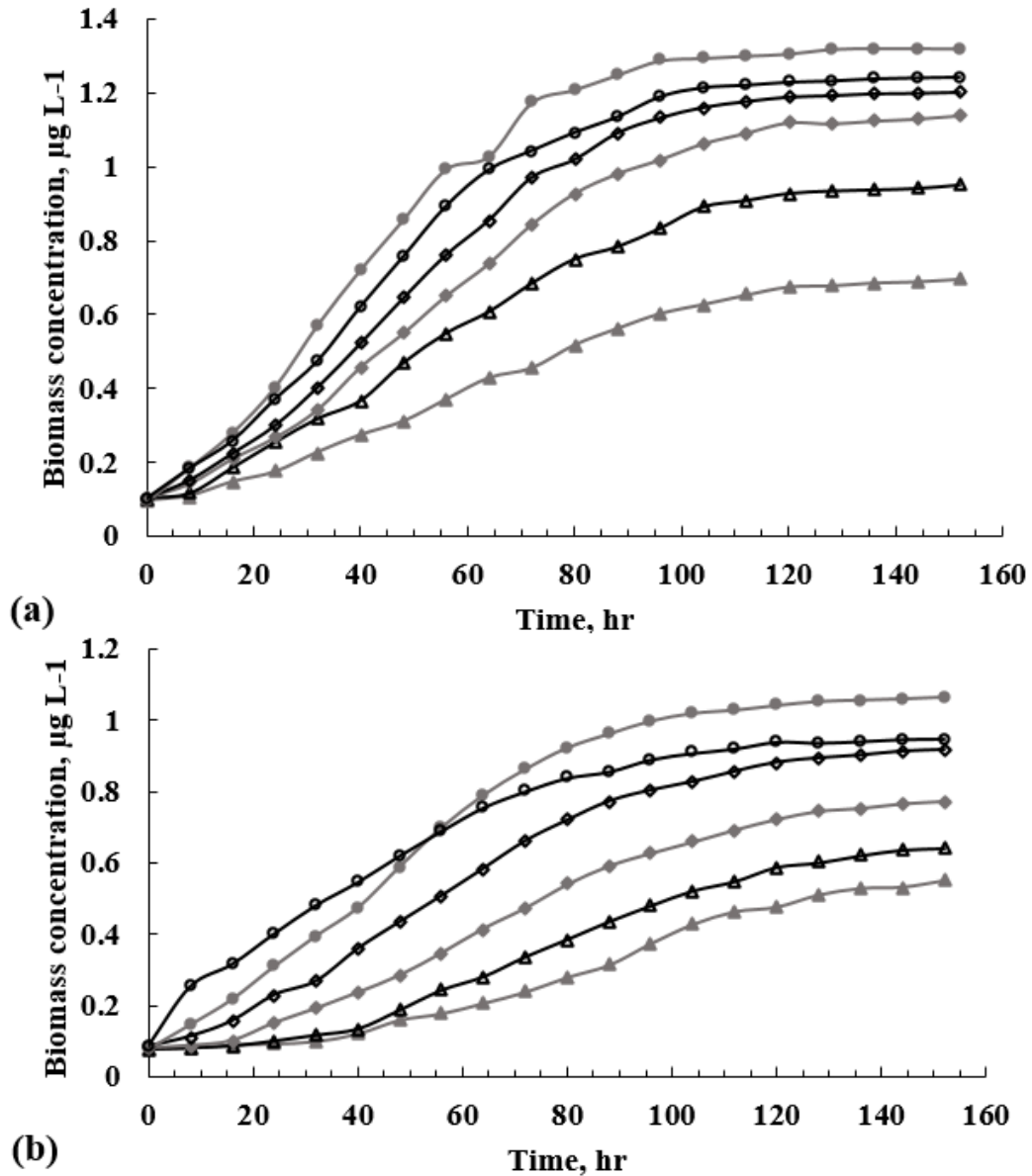
220 where  $x$  is the vector of variables containing the chemicals and algal species in the model,  $\hat{x}$   
 221 is the measured states,  $p$  is the vector of the model parameters to be determined,  $\alpha$  is the

222 weighting factor, and  $N$  is the number of experimental data points. This optimisation problem  
223 is solved in a multi-start framework from different points in the parameter-space to obtain a  
224 high-quality solution. Parameter estimation was performed using the state-of-the-art interior  
225 point nonlinear optimisation solver IPOPT. The implementation in this work was programmed  
226 in the Python optimisation environment Pyomo<sup>37</sup>. Kinetic model simulation was conducted in  
227 the commercial software Mathematica<sup>TM</sup> 11.0.

## 228 **RESULTS & DISCUSSION**

### 229 **Effects of light intensity and temperature on biomass growth**

230 Both biomass growth rates and total biomass concentration increased with increasing incident  
231 light intensity from 20  $\mu\text{E}$  to 60  $\mu\text{E}$ , with a maximum at 100  $\mu\text{E}$ , beyond which a decrease was  
232 observed (Fig. 1a). This indicates that photoinhibition becomes severe when light intensity  
233 reaches 300  $\mu\text{E}$ , and optimal light intensity for cell growth may fall within the range between  
234 100  $\mu\text{E}$  to 300  $\mu\text{E}$ . However, it should be noted that as a result of light attenuation, caused by  
235 light absorption and cell shading, incident and local light intensities within a PBR can be  
236 substantially different<sup>28,34,38</sup>. Thus, the optimal light intensity for the current mutant will be  
237 estimated further by the kinetic model.



238

239 Figure 1: Growth of *C. reinhardtii* bisabolene production strain under different operating

240 conditions. (a): biomass growth at 30 °C with incident light intensities of 20  $\mu\text{E}$  (grey triangles),

241 40  $\mu\text{E}$  (open triangles), 60  $\mu\text{E}$  (grey diamonds), 80  $\mu\text{E}$  (open diamonds), 100  $\mu\text{E}$  (grey circles)

242 and 300  $\mu\text{E}$  (open circles); (b): biomass growth with light intensity of 60  $\mu\text{E}$  at temperatures of

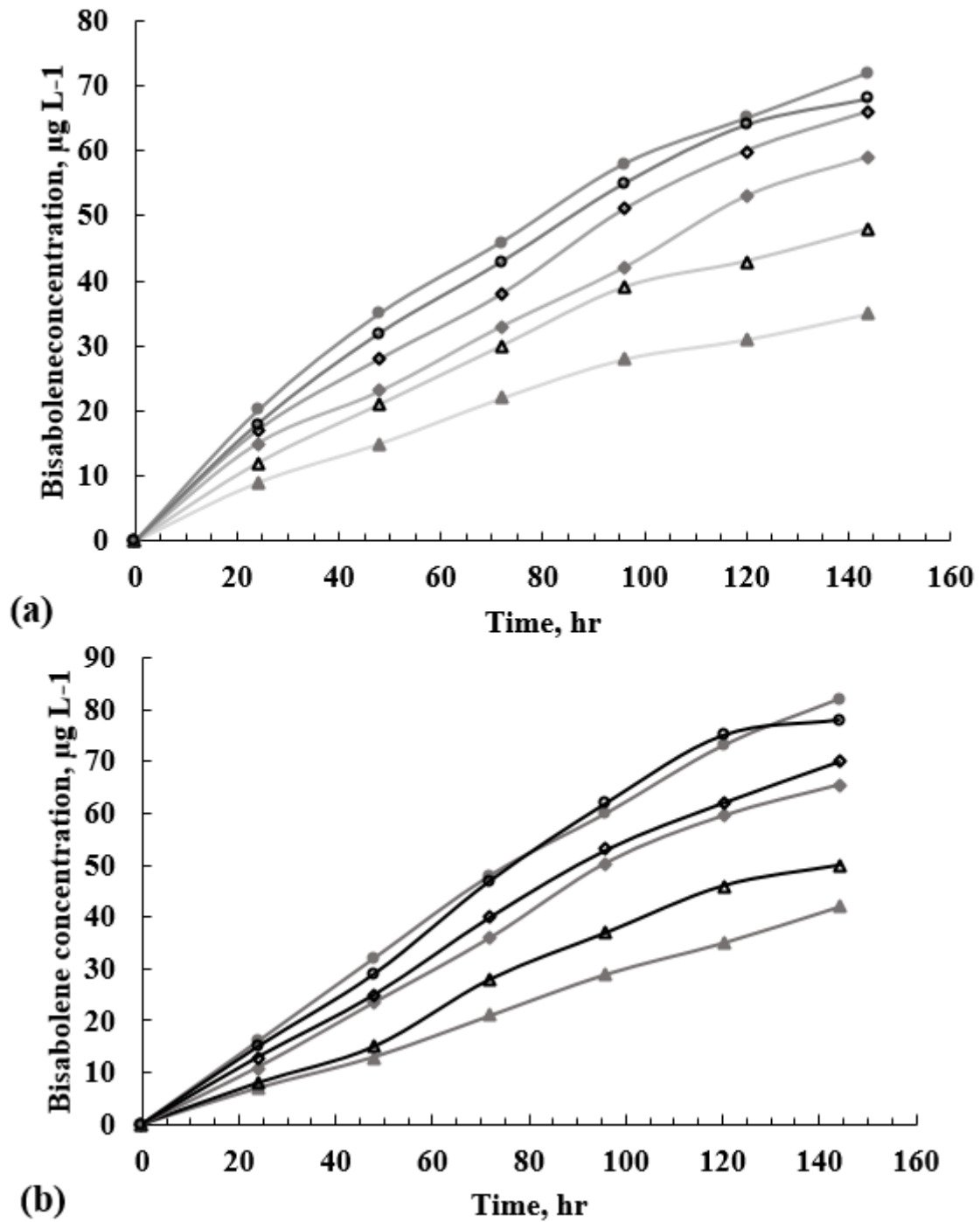
243 22 °C (grey triangles), 24 °C (open triangles), 26 °C (grey diamonds), 28 °C (open diamonds),

244 30 °C (grey circles) and 32 °C (open circles).

245 The biomass growth rate was also found to be enhanced when the cultivation temperature was  
246 increased from 22 °C to 30 °C, beyond which a decrease in biomass growth rate and final  
247 biomass concentration was observed (Fig. 1b). In addition, the close match of the final biomass  
248 concentrations at 28 °C and 32 °C suggests that the culture temperature should be controlled  
249 within this range. Indeed, the optimal cultivation temperature for *C. reinhardtii* is known to  
250 fall within this range<sup>39</sup>.

### 251 **Effects of light intensity and temperature on bisabolene yields**

252 Bisabolene concentrations were found to increase even after the culture reached stationary  
253 phase (~100 hours), regardless of the light intensity or temperature (Fig. 2). This indicates that  
254 bisabolene is synthesised from this strain at different growth phases and is not solely dependent  
255 on cell growth. It can also be seen that similar to biomass growth, bisabolene production  
256 reached a maximum at 100 µE (Fig. 2a) and 30 °C (Fig. 2b), respectively. Bisabolene  
257 production followed similar trends with respect to cell accumulation and effects of temperature  
258 and light are almost identical compared to those on cell growth.



259

260

261

262

263

Figure 2: Bisabolene yields under different operating conditions. (a): bisabolene yields at 30 °C with incident light intensities of 20  $\mu\text{E}$  (grey triangles), 40  $\mu\text{E}$  (open triangles), 60  $\mu\text{E}$  (grey diamonds), 80  $\mu\text{E}$  (open diamonds), 100  $\mu\text{E}$  (grey circles) and 300  $\mu\text{E}$  (open circles); (b): bisabolene yields with light intensity of 60  $\mu\text{E}$  at temperatures of 22 °C (grey triangles), 24 °C

264 (open triangles), 26 °C (grey diamonds), 28 °C (open diamonds), 30 °C (grey circles) and 32 °C  
265 (open circles).

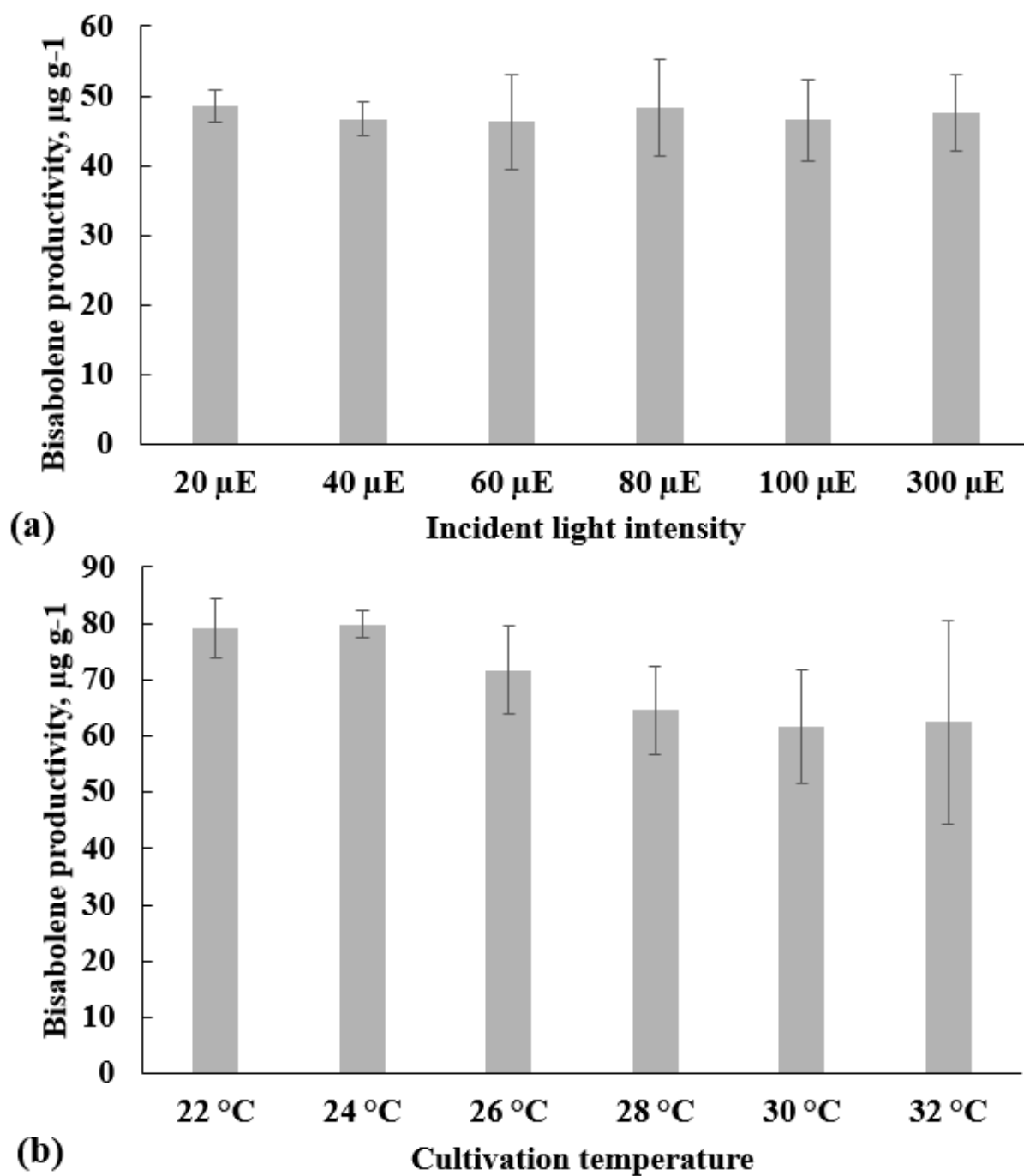
266 The above observations do not, however, imply that the optimal conditions for algal biomass  
267 growth and bisabolene synthesis are the same. Total volumetric bisabolene production ( $\mu\text{g L}^{-1}$   
268 <sup>1</sup>) is the product of biomass concentration ( $\text{g L}^{-1}$ ) and the biomass-specific bisabolene  
269 productivity ( $\mu\text{g g}^{-1}$ ). As a result, the total volumetric production of bisabolene can be increased  
270 at conditions favouring biomass growth, even if the biomass-specific bisabolene productivity  
271 is below optimal. Inefficient bisabolene production per biomass reduces the carbon and energy  
272 utilisation efficiency for bisabolene production, as well as increasing the consumption of  
273 nitrogen, phosphorus and minerals for undesired biomass production. Hence, effects of light  
274 intensity and temperature on bisabolene synthesis were further explored.

275 The comparison of the specific bisabolene productivities ( $\mu\text{g g}^{-1}$ ) at the different light  
276 intensities shows little variation across the entire measurement range, suggesting that  
277 bisabolene synthesis is not directly linked to the change of light intensity (Table 2 and Fig.  
278 3(a)). It was previously determined that day-night cycles could result in increased volumetric  
279 bisabolene productivities <sup>21</sup>. However, this effect was determined to be due to a prolonged  
280 exponential phase, rather than a difference at a cellular level, and supports the current finding  
281 that light intensity is not coupled to increases in the biomass-specific bisabolene productivity.  
282 Moreover, although the sesquiterpenoid pathway uses the same precursors as pigment  
283 biosynthesis, it is not directly coupled to photosynthesis. The precursor for bisabolene  
284 production, farnesyl pyrophosphate (FPP), is found in the cytoplasm rather than the chloroplast



285 and is used for sterol biosynthesis, rather than light harvesting, further supporting this finding

286 <sup>14,21</sup>.



287

288 Figure 3: Biomass-specific, averaged bisabolene production under different operating

289 conditions. (a): Effect of incident light intensity at 30 °C; (b): Effect of cultivation temperature

290 at 60  $\mu\text{E}$ .

291 Table 2: Biomass-specific, averaged bisabolene production ( $\mu\text{g g}^{-1}_{\text{DBM}}$ ) under different  
 292 operating conditions

| Different light intensity ( $\mu\text{E}$ ), temperature fixed at 30 °C. |                |                |                |                |                 |                 |
|--|----------------|----------------|----------------|----------------|-----------------|-----------------|
| Light  | 20             | 40             | 60             | 80             | 100             | 300             |
| Productivity   | $48.5 \pm 2.3$ | $46.7 \pm 2.5$ | $46.3 \pm 6.7$ | $48.3 \pm 7.0$ | $46.5 \pm 5.9$  | $47.6 \pm 5.4$  |
| Different temperature (°C), light intensity fixed at 60 $\mu\text{E}$    |                |                |                |                |                 |                 |
| Temperature  | 22             | 24             | 26             | 28             | 30              | 32              |
| Productivity   | $79.1 \pm 5.3$ | $79.9 \pm 2.3$ | $71.7 \pm 7.8$ | $64.7 \pm 7.8$ | $61.5 \pm 10.0$ | $62.4 \pm 18.0$ |

293 It should be noted, however, that the current set of experiments was conducted under  
 294 mixotrophic conditions with acetate in the growth medium. In mixotrophic conditions both  
 295 mitochondrial respiration and photosynthesis act synergistically to increase culture growth  
 296 rates. Indeed, in a previous study with the same host strain engineered to produce patchoulol,  
 297 biomass and patchoulol yields were enhanced by the addition of acetate, although patchoulol  
 298 production continued to increase even after the acetate had been depleted<sup>14</sup>. As sesquiterpene  
 299 metabolism (bisabolene) is related to mitochondrial respiration rather than light harvesting,  
 300 even in the absence of acetate, light intensity is unlikely to have any effect on the biomass-  
 301 specific bisabolene productivities. This is different to the production of algal biohydrogen and  
 302 biolipid, which are known to be limited by light related metabolic reactions associated with the  
 303 photosynthetic electron transport chain<sup>40,41</sup>.

304 In contrast to the effect of incident light, cellular bisabolene production is significantly affected  
 305 by the culture temperature from 22 °C to 30 °C (Table 2 and Fig. 3(b)), particularly during the

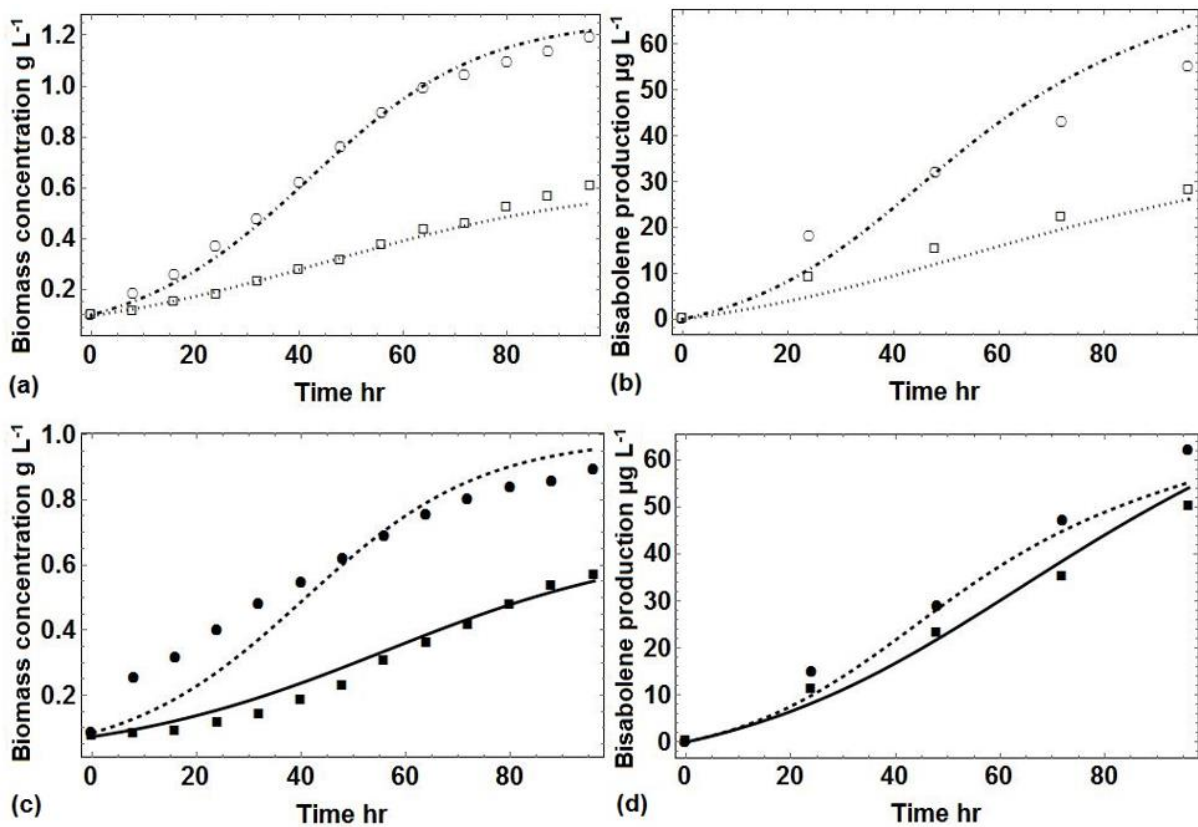
306 early growth stage. A remarkable increase of 23.0% (from 61.5  $\mu\text{g g}^{-1}$  to 79.9  $\mu\text{g g}^{-1}$ ) was  
307 observed when the temperature decreased from 30 °C to 24 °C. This clearly indicates that the  
308 optimal temperature for bisabolene synthesis is different from that for algal biomass growth,  
309 and to maximise the bisabolene synthesis rate the cultivation temperature should be maintained  
310 below 28 °C. In addition, it can be concluded that the trend of cellular bisabolene production  
311 with respect to temperature, *i.e.* decreasing from 24 °C to 30 °C, is exactly opposite to that of  
312 cell growth. In fact, it is the reduction in cell growth which may directly contribute to increasing  
313 the specific bisabolene productivity by prolonging the growth phases (Fig. 1(b)). A similar  
314 effect was observed when cultivating the strain under light-dark cycles, which as expected  
315 slowed down growth, final bisabolene titres were increased by up to 50%.

316 Interestingly, the calculated bisabolene productivities for the low temperature experiments  
317 were much more consistent over the whole growth cycle than the higher temperature  
318 experiments, which are significantly reduced in the growth phases and only recovered in the  
319 stationary phase. Indeed, the application of a dodecane overlay for the *in-situ* recovery of  
320 bisabolene increased the overall product yield more than five-fold compared to cultivation  
321 without dodecane <sup>21</sup>. Consequently, further studies should be conducted to test the online  
322 recovery of bisabolene, to investigate whether overall productivities could be increased. In all  
323 cases, to maximise the solar conversion efficiency towards bisabolene and maintain high  
324 biofuel production rates, it is vital to identify operating conditions under which the culture  
325 volumetric bisabolene productivity is maintained high. As a result, an accurate dynamic model

326 capable of simulating both algal biomass growth and bisabolene production becomes an  
327 efficient tool to resolve this challenge.

### 328 **Results of kinetic model construction**

329 The current parameter estimation results are listed in Table 3. From the table, it is seen that  
330 bubble scattering coefficient was estimated to be 0, suggesting its effect on light transmission  
331 is negligible compared to cell absorption (Table 3). Comparing the model results to the  
332 experimental data shows that the current model provides a good representation of the dynamic  
333 trend of both biomass growth and bisabolene production (Fig. 4). Except of a slight  
334 underestimation of biomass concentration at the beginning period of Experiment 4, the model  
335 maximum fitting error is 13.9% occurring at the 96<sup>th</sup> hour for bisabolene production in  
336 Experiment 2, with an average fitting error around 5% for these four experiments.



337

338 Figure 4: Dynamic model simulation results for biomass growth (a, c) and bisabolene  
 339 production (b, d): Dotted line: model fitting results for Experiment 1 (open squares); Dot-  
 340 dashed line: model fitting results for Experiment 2 (open circles); Thick line: model fitting  
 341 results for Experiment 3 (filled squares); Dashed line: model fitting results for Experiment 4  
 342 (filled circles).

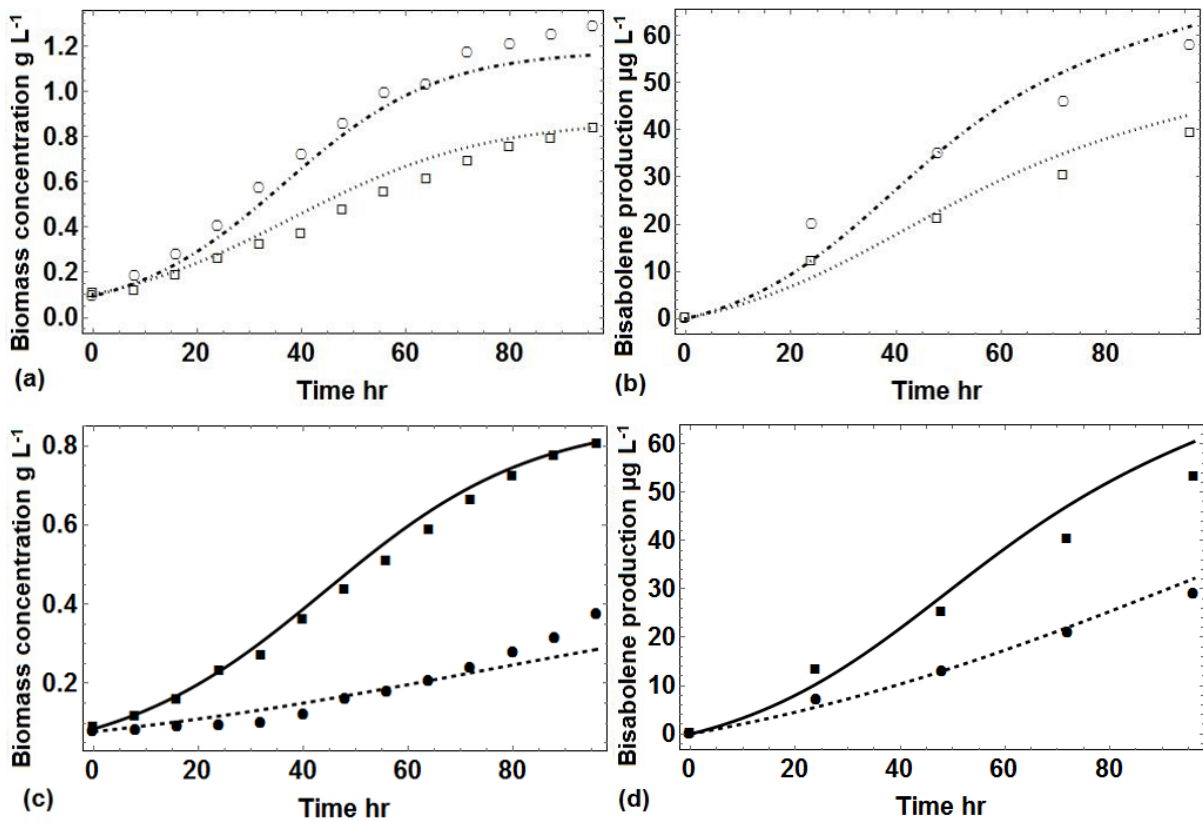
343 Table 3: Parameter estimation results for the current dynamic model

| Parameter                                   | Value                  | Parameter                                       | Value |
|---|------------------------|---|-------|
| $\mu$ , h <sup>-1</sup>                     | 0.304                  | $E_a$ , kJ mol <sup>-1</sup>                    | 144.0 |
| $\mu_d$ , L g <sup>-1</sup> h <sup>-1</sup> | $5.075 \times 10^{-2}$ | $E_b$ , kJ mol <sup>-1</sup>                    | 343.9 |
| $k_s$ , $\mu$ E                             | 34.92                  | $T_a$ , K                                       | 306.7 |
| $k_i$ , $\mu$ E                             | 441.2                  | $T_b$ , K                                       | 307.1 |
| $\tau$ , L g <sup>-1</sup> m <sup>-1</sup>  | 0.0339                 | $Y_1$ , $\mu$ g g <sup>-1</sup>                 | 326.7 |
| $K_a$ , m <sup>-1</sup>                     | 0.0                    | $Y_2$ , $\mu$ g g <sup>-1</sup> h <sup>-1</sup> | 1.758 |
| $\alpha$ , --                               | 0.474                  |   |       |

#### 344 **Dynamic model predictive capability**

345 To facilitate the process design, optimisation, and control for future algal bisabolene  
 346 production, it is essential that the model is capable of accurately predicting the dynamic  
 347 performance of an unknown process. Therefore, the predictive capability of the current model  
 348 was verified against the four test experiments executed under different operating conditions  
 349 (Fig. 5). In most cases, the error was less than 5%, with a maximum error of 20.3%, at the 96<sup>th</sup>  
 350 hour for biomass concentration in Test 4, suggesting that the model effectively predicts

351 biomass growth and bisabolene production throughout the experiments even at the most severe  
 352 conditions (*e.g.* Test 4 where temperature was the lowest). Hence, the model has great  
 353 predictive capability and can be used for further process optimisation and control.



354  
 355 Figure 5: Dynamic model prediction results for biomass growth (a, c) and bisabolene  
 356 production (b, d): Dotted line: model prediction results for Test 1 (open squares); Dot-dashed  
 357 line: model prediction results for Test 2 (open circles); Thick line: model prediction results for  
 358 Test 3 (filled squares); Dashed line: model prediction results for Test 4 (filled circles).

### 359 Impact of light attenuation on mutant growth

360 Based on the model, the impact of light attenuation on biomass growth was analysed (Table  
 361 4). It was found that unlike previous results for cyanobacteria cultures<sup>28</sup>, the effect of  
 362 microalgal cell absorption on local light intensities within the PBR was relatively low. Even at  
 363 the maximum algal biomass concentrations achieved in this study (1.3 g L<sup>-1</sup>), the average light

364 intensity in the PBR was 60.6% of the incident light intensity, whilst the lowest local light  
 365 intensity at the reactor front surface remained at 32.7% of the incident light intensity. This  
 366 conclusion is consistent with the recent study in which a thorough comparison on light  
 367 attenuation induced by different species, in particular green alga *C. reinhardtii* and  
 368 cyanobacterium *Cyanothece* sp., was presented <sup>42</sup>. The study declared that compared to  
 369 cyanobacteria, cell absorption caused by green algae is much milder in a laboratory scale PBR,  
 370 and may not be the primary limiting factor for cell growth and biorenewables synthesis until  
 371 the very end of the experiment.

372 Table 4: Average light intensity (% incident light intensity) at different biomass concentration

| Algal biomass concentration | Lab-scale (width 0.025 m) | Pilot scale (width 0.25 m) |
|-----------------------------|---------------------------|----------------------------|
| 0.1 g L <sup>-1</sup>       | 95.9%                     | 67.5%                      |
| 0.5 g L <sup>-1</sup>       | 81.5%                     | 23.3%                      |
| 0.9 g L <sup>-1</sup>       | 70.0%                     | 13.1%                      |
| 1.3 g L <sup>-1</sup>       | 60.6%                     | 9.1%                       |

373 However, once the reactor is scaled up into a pilot system, and the width of the flat-plate PBR  
 374 is increased from 0.025 m to 0.25 m, the current simulation results show that the average light  
 375 intensity in the reactor decreases dramatically. For instance, at a cell concentration of 0.5 g L<sup>-1</sup>  
 376 <sup>1</sup> average light intensity decreases by 76.7% compared to the incident light intensity (Table 4),  
 377 and local light intensities at the reactor front drops to zero based on the current calculation if  
 378 illumination is provided only from the back. This indicates that once the system is scaled up,

379 the primary challenge for biomass growth and bioproducts synthesis may switch from intrinsic  
380 limits (*e.g.* metabolic activities) to process scale-up issues (*e.g.* reactor design).

### 381 **Optimal light intensity and temperature**

382 Finally, as the effect of light attenuation was minor in the current experiments, optimal light  
383 intensity for the mutant growth should be close to the measured optimum (100  $\mu\text{E}$ ). By taking  
384 into account light attention, optimal light intensity and temperature for algal cell growth were  
385 estimated to be 124.2  $\mu\text{E}$  and 30.8  $^{\circ}\text{C}$ , respectively. As the effect of light intensity on bisabolene  
386 synthesis was also found to be minor, optimal light intensity for bisabolene production could  
387 be fixed same as that for biomass growth. Nonetheless, to balance the temperature trade-off  
388 effect between cell growth and bisabolene synthesis, optimal temperature for total volumetric  
389 bisabolene production was estimated to be 30.9  $^{\circ}\text{C}$ . The similarities in the optimal temperatures  
390 for biomass growth and total bisabolene production suggest that total bisabolene production is  
391 dominated by biomass concentration rather than high biomass-specific bisabolene productivity.  
392 As a result, a combination of 124.2  $\mu\text{E}$  and 30.9  $^{\circ}\text{C}$  can be considered as the optimal operating  
393 condition for continuous algal bisabolene production.

### 394 **CONCLUSION**

395 In this study, effects of light intensity and temperature on both the modified *Chlamydomonas*  
396 *reinhardtii* UVM4 biomass growth and bisabolene (excreted biofuel) synthesis were  
397 investigated. Through experimental analysis and dynamic modelling, the current research  
398 found that under mixotrophic growth conditions, bisabolene was partially expressed  
399 independent of biomass growth, resulting in continued production during the stationary phase.



400 Whilst light intensity had minimal effect on the biomass-specific bisabolene productivity,  
401 bisabolene formation was strongly favoured at low and high temperatures, at which biomass  
402 growth was reduced. Nevertheless, as the overall bisabolene production is proportional to the  
403 biomass concentration, the optimal temperature for bisabolene productivity deviates only  
404 slightly from that for biomass growth. It is therefore concluded that optimal conditions for cell  
405 growth and biofuel production are different, and robust bioprocess real-time optimisation  
406 strategies should be adopted to guarantee high resources conversion efficiency when scaling  
407 up this system. This research, therefore, paves the way for future studies of sustainable excreted  
408 algal biofuels and mutant development.

#### 409 **Acknowledgments**

410 This project has received funding from the European Union's Horizon 2020 research and  
411 innovation programme under grant agreement No 640720. This project has also received  
412 funding from the EPSRC project (EP/P016650/1, P65332). Irina acknowledges funding from  
413 the Ministry of Higher Education, Malaysia and University Putra Malaysia. The bisabolene  
414 excreting mutant of *Chlamydomonas reinhardtii* was developed by Julian Wichmann and Kyle  
415 J. Lauersen working in the group of Olaf Kruse at Universität Bielefeld, Germany.

#### 416 **References**

- 417 1. Radakovits R, Jinkerson RE, Darzins A, Posewitz MC. Genetic engineering of algae for  
418 enhanced biofuel production. *Eukaryot Cell*. 2010;9(4):486-501.  
419 doi:10.1128/EC.00364-09.
- 420 2. Parmar A, Singh NK, Pandey A, Gnansounou E, Madamwar D. Cyanobacteria and

- 421 microalgae: A positive prospect for biofuels. *Bioresour Technol.* 2011;102(22):10163-  
422 10172. doi:10.1016/j.biortech.2011.08.030.
- 423 3. Chisti Y. Constraints to commercialization of algal fuels. *J Biotechnol.*  
424 2013;167(3):201-214. doi:10.1016/j.jbiotec.2013.07.020.
- 425 4. Rawat I, Ranjith Kumar R, Mutanda T, Bux F. Biodiesel from microalgae: A critical  
426 evaluation from laboratory to large scale production. *Appl Energy.* 2013;103(0):444-  
427 467. doi:10.1016/j.apenergy.2012.10.004.
- 428 5. Mikkonen S, Hartikka T, Kuronen M, Saikkonen P. *HVO, Hydrotreated Vegetable Oil*  
429 *- a Premium Renewable Biofuel for Diesel Engines.*; 2012.
- 430 6. Wagner J, Bransgrove R, Beacham TA, Allen M, Meixner K, Drosch B, Ting V, Chuck  
431 C. Co-production of bio-oil and propylene through the hydrothermal liquefaction of  
432 polyhydroxybutyrate producing cyanobacteria. *Bioresour Technol.* 2016;207:166-174.  
433 doi:10.1016/j.biortech.2016.01.114.
- 434 7. Wagner JL, Le CD, Ting VP, Chuck CJ. Design and operation of an inexpensive,  
435 laboratory-scale, continuous hydrothermal liquefaction reactor for the conversion of  
436 microalgae produced during wastewater treatment. *Fuel Process Technol.*  
437 2017;165:102-111. doi:10.1016/j.fuproc.2017.05.006.
- 438 8. Tian C, Li B, Liu Z, Zhang Y, Lu H. Hydrothermal liquefaction for algal biorefinery: A  
439 critical review. *Renew Sustain Energy Rev.* 2014;38:933-950.  
440 doi:10.1016/j.rser.2014.07.030.
- 441 9. Kato A, Takatani N, Ikeda K, Maeda S, Omata T. Removal of the product from the

- 442 culture medium strongly enhances free fatty acid production by genetically engineered  
443 *Synechococcus elongatus*. *Biotechnol Biofuels*. 2017;10(1):141. doi:10.1186/s13068-  
444 017-0831-z.
- 445 10. Pade N, Mikkat S, Hagemann M. Ethanol, glycogen and glucosylglycerol represent  
446 competing carbon pools in ethanol-producing cells of *Synechocystis* sp. PCC 6803  
447 under high-salt conditions. *Microbiology*. 2017;163(3):300-307.  
448 doi:10.1099/mic.0.000433.
- 449 11. Hirokawa Y, Dempo Y, Fukusaki E, Hanai T. Metabolic engineering for isopropanol  
450 production by an engineered cyanobacterium, *Synechococcus elongatus* PCC 7942,  
451 under photosynthetic conditions. *J Biosci Bioeng*. 2017;123(1):39-45.  
452 doi:10.1016/j.jbiosc.2016.07.005.
- 453 12. Halfmann C, Gu L, Gibbons W, Zhou R. Genetically engineering cyanobacteria to  
454 convert CO<sub>2</sub>, water, and light into the long-chain hydrocarbon farnesene. *Appl*  
455 *Microbiol Biotechnol*. 2014;98(23):9869-9877. doi:10.1007/s00253-014-6118-4.
- 456 13. del Rio-Chanona EA, Zhang D, Shah N. Sustainable biopolymer synthesis via  
457 superstructure and multiobjective optimization. *AIChE J*. July 2017.  
458 doi:10.1002/aic.15877.
- 459 14. Lauersen KJ, Baier T, Wichmann J, Wördenweber R, Mussnug JH, Hübner W, Huser  
460 T, Kruse O. Efficient phototrophic production of a high-value sesquiterpenoid from the  
461 eukaryotic microalga *Chlamydomonas reinhardtii*. *Metab Eng*. 2016;38:331-343.  
462 doi:10.1016/j.ymben.2016.07.013.

- 463 15. Misawa N. Pathway engineering for functional isoprenoids. *Curr Opin Biotechnol.*  
464 2011;22(5):627-633. doi:10.1016/j.copbio.2011.01.002.
- 465 16. Bohlmann J, Crock J, Jetter R, Croteau R. Terpenoid-based defenses in conifers: cDNA  
466 cloning, characterization, and functional expression of wound-inducible (E)-  
467 bisabolene synthase from grand fir (*Abies grandis*). *Proc Natl Acad Sci.*  
468 1998;95(12):6756-6761. doi:10.1073/pnas.95.12.6756.
- 469 17. Peralta-Yahya PP, Ouellet M, Chan R, Mukhopadhyay A, Keasling JD, Lee TS.  
470 Identification and microbial production of a terpene-based advanced biofuel. *Nat*  
471 *Commun.* 2011;2:483. doi:10.1038/ncomms1494.
- 472 18. Baba M, Shiraiwa Y. Biosynthesis of lipids and hydrocarbons in algae. In: Dubinsky Z,  
473 ed. *Photosynthesis.* ; 2013:321-355. doi:10.5772/56413.
- 474 19. Melis A. Carbon partitioning in photosynthesis. *Curr Opin Chem Biol.* 2013;17(3):453-  
475 456. doi:10.1016/j.cbpa.2013.03.010.
- 476 20. Davies FK, Work VH, Beliaev AS, Posewitz MC. Engineering Limonene and  
477 Bisabolene Production in Wild Type and a Glycogen-Deficient Mutant of  
478 *Synechococcus* sp. PCC 7002. *Front Bioeng Biotechnol.* 2014;2.  
479 doi:10.3389/fbioe.2014.00021.
- 480 21. Wichmann J, Baier T, Wentnagel E, Lauersen KJ, Kruse O. Tailored carbon partitioning  
481 for phototrophic production of (E)- $\alpha$ -bisabolene from the green microalga  
482 *Chlamydomonas reinhardtii*. *Metab Eng.* 2018;45:211-222.  
483 doi:10.1016/j.ymben.2017.12.010.

- 484 22. Scaife MA, Nguyen GTDT, Rico J, Lambert D, Helliwell KE, Smith AG. Establishing  
485 *Chlamydomonas reinhardtii* as an industrial biotechnology host. *Plant J.*  
486 2015;82(3):532-546. doi:10.1111/tpj.12781.
- 487 23. Neupert J, Karcher D, Bock R. Generation of *Chlamydomonas* strains that efficiently  
488 express nuclear transgenes. *Plant J.* 2009;57(6):1140-1150. doi:10.1111/j.1365-  
489 313X.2008.03746.x.
- 490 24. Gorman DS, Levine RP. Photosynthetic Electron Transport Chain of *Chlamydomonas*  
491 *reinhardtii*. V. Purification and Properties of Cytochrome 553 and Ferredoxin. *Plant*  
492 *Physiol.* 1966;41(0):1643-1647.
- 493 25. Tamburic B, Zemichael FW, Crudge P, Maitland G, Hellgardt K. Design of a novel flat-  
494 plate photobioreactor system for green algal hydrogen production. *Int J Hydrogen*  
495 *Energy.* 2011;36(11):6578-6591. doi:10.1016/j.ijhydene.2011.02.091.
- 496 26. Jing K, Tang Y, Yao C, del Rio-Chanona EA, Ling X, Zhang D. Overproduction of L-  
497 tryptophan via simultaneous feed of glucose and anthranilic acid from recombinant  
498 *E.coli* W3110: kinetic modelling and process scale-up. *Biotechnol Bioeng.* August 2017.  
499 doi:10.1002/bit.26398.
- 500 27. Dechatiwongse P, Srisamai S, Maitland G, Hellgardt K. Effects of light and temperature  
501 on the photoautotrophic growth and photoinhibition of nitrogen-fixing cyanobacterium  
502 *Cyanothece* sp. ATCC 51142. *Algal Res.* 2014;5(0):103-111.  
503 doi:10.1016/j.algal.2014.06.004.
- 504 28. Zhang D, Dechatiwongse P, del Rio-Chanona E a., Maitland GC, Hellgardt K,

- 505 Vassiliadis VS. Modelling of light and temperature influences on cyanobacterial growth  
506 and biohydrogen production. *Algal Res.* 2015;9:263-274.  
507 doi:10.1016/j.algal.2015.03.015.
- 508 29. Béchet Q, Shilton A, Guieysse B. Modeling the effects of light and temperature on algae  
509 growth: State of the art and critical assessment for productivity prediction during  
510 outdoor cultivation. *Biotechnol Adv.* 2013;31(8):1648-1663.  
511 doi:10.1016/j.biotechadv.2013.08.014.
- 512 30. del Rio-Chanona EA, Ahmed N rashid, Zhang D, Lu Y, Jing K. Kinetic modeling and  
513 process analysis for *Desmodesmus* sp. lutein photo-production. *AIChE J.*  
514 2017;63(7):2546-2554. doi:10.1002/aic.15667.
- 515 31. Mu Y, Yang H-Y, Wang Y-Z, He C-S, Zhao Q-B, Wang Y, Yu H-Q. The maximum  
516 specific hydrogen-producing activity of anaerobic mixed cultures: definition and  
517 determination. *Sci Rep.* 2015;4(1):5239. doi:10.1038/srep05239.
- 518 32. Río E Del, Acién FG, García-Malea MC, Rivas J, Molina-Grima E, Guerrero MG.  
519 Efficient one-step production of astaxanthin by the microalga *Haematococcus pluvialis*  
520 in continuous culture. *Biotechnol Bioeng.* 2005;91(7):808-815. doi:10.1002/bit.20547.
- 521 33. Dechatiwongse P, Maitland G, Hellgardt K. Demonstration of a two-stage  
522 aerobic/anaerobic chemostat for the enhanced production of hydrogen and biomass from  
523 unicellular nitrogen-fixing cyanobacterium. *Algal Res.* 2015;10:189-201.  
524 doi:10.1016/j.algal.2015.05.004.
- 525 34. del Rio-Chanona EA, Zhang D, Xie Y, Manirafasha E, Jing K. Dynamic Simulation and

- 526 Optimization for *Arthrospira platensis* Growth and C-Phycocyanin Production. *Ind Eng*  
527 *Chem Res.* 2015;54(43):10606-10614. doi:10.1021/acs.iecr.5b03102.
- 528 35. Kameswaran S, Biegler LT. Convergence rates for direct transcription of optimal control  
529 problems using collocation at Radau points. *Comput Optim Appl.* 2008;41(1):81-126.  
530 doi:10.1007/s10589-007-9098-9.
- 531 36. Faber R, Li P, Wozny G. Sequential Parameter Estimation for Large-Scale Systems with  
532 Multiple Data Sets. 1. Computational Framework. *Ind Eng Chem Res.*  
533 2003;42(23):5850-5860. doi:10.1021/ie030296s.
- 534 37. del Rio-Chanona EA, Dechatiwongse P, Zhang D, Maitland G, Hellgardt K, Arellano-  
535 Garcia H, Vassiliadis V. Optimal Operation Strategy for Biohydrogen Production. *Ind*  
536 *Eng Chem Res.* 2015;54(24):6334-6343. doi:10.1021/acs.iecr.5b00612.
- 537 38. Zhang D, Wan M, del Rio-Chanona EA, Huang J, Wang W, Li Y, Vassiliadis V.  
538 Dynamic modelling of *Haematococcus pluvialis* photoinduction for astaxanthin  
539 production in both attached and suspended photobioreactors. *Algal Res.* 2016;13:69-78.  
540 doi:10.1016/j.algal.2015.11.019.
- 541 39. Copyright. In: *The Chlamydomonas Sourcebook*. Elsevier; 2009:iii. doi:10.1016/B978-  
542 0-12-370873-1.00059-9.
- 543 40. Johnson X, Alric J. Central Carbon Metabolism and Electron Transport in  
544 *Chlamydomonas reinhardtii*: Metabolic Constraints for Carbon Partitioning between Oil  
545 and Starch. *Eukaryot Cell.* 2013;12(6):776-793. doi:10.1128/EC.00318-12.
- 546 41. Cardol P, Forti G, Finazzi G. Regulation of electron transport in microalgae. *Biochim*

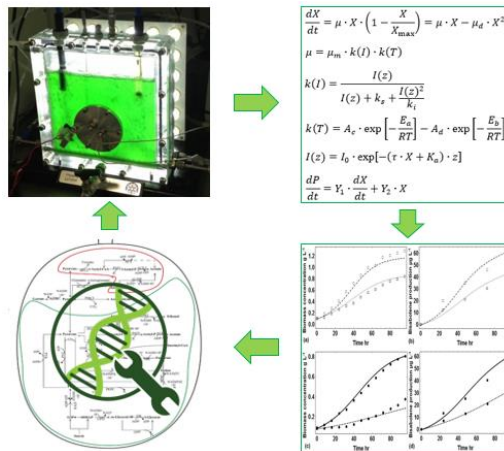
547 *Biophys Acta - Bioenerg.* 2011;1807(8):912-918. doi:10.1016/j.bbabi.2010.12.004.

548 42. Zhang D, Chanona EAD-R, Vassiliadis VS, Tamburic B. Analysis of green algal growth  
549 via dynamic model simulation and process optimization. *Biotechnol Bioeng.*  
550 2015;112(10). doi:10.1002/bit.25610.

551

552

### Table of Contents



553